Lanthanide-Doped Nanoparticles with Excellent Luminescent Properties in Organic Media

Jan W. Stouwdam, Gerald A. Hebbink, Jurriaan Huskens, and Frank C. J. M. van Veggel*,†

Laboratories of Supramolecular Chemistry and Technology & MESA+ Research Institute, University of Twente, P.O. Box 217, 7500 AE Enschede, The Netherlands

Received June 16, 2003. Revised Manuscript Received September 9, 2003

Surface-coated nanoparticles of LaF_3 and $LaPO_4$ doped with the luminescent trivalent lanthanide ions Eu^{3+}, Nd^{3+}, Er^{3+}, Pr^{3+}, Ho^{3+}, and Yb^{3+} have been prepared. These ions emit in the visible and in the near-infrared part of the electromagnetic spectrum. The ions Nd^{3+}, Er^{3+}, Pr^{3+}, and Ho^{3+} are the main focus in this research because they show emissions in telecommunication windows. The Yb^{3+} ion is of interest because it can be used as a sensitizer for Er^{3+}. The Eu^{3+} ion has been used as a probe for the structural environment of the luminescent ion. It is shown that these lanthanide ions are incorporated in the inorganic host of the particles and that the particles are dispersable in organic solvents. The luminescent lifetimes of the ions are increased by orders of magnitude compared to organic complexes, with values ranging from several microseconds for Pr^{3+} and Ho^{3+}, up to about 200 μs for Nd^{3+}, and 1 ms for Er^{3+}. This increase in the luminescence lifetime is indicative of an effective shielding of the lanthanide ions from nonradiative decay of the excited state by the high-energy vibrations of the solvents and the coordinated organic ligands. A model is proposed to describe the nonexponential behavior of the luminescence decay by quenching from outside the particle. It uses two fit parameters, k_R, a parameter describing the luminescence decay rate in the absence of surface quenching, and C, a parameter describing the sensitivity toward quenching. Using this model, the luminescence decays can be fitted very well, and factors influencing the luminescence lifetime like concentration quenching and solvent effects can be described accurately.

Introduction

Nanoparticles coated with organic surfactants are an interesting new class of materials that emerged over the past decade.[1,2] The surfactant coating protects the particles against aggregation, controls the growth of the particles, and gives them dispersability in organic solvents. Luminescent nanoparticles are an important class of these nanoparticles because they open a way to use the luminescence of inorganic compounds in an organic environment. Inorganic compounds doped with lanthanide ions are widely used as the luminescent material in lighting and displays,[3] optical amplifiers,[4] and lasers.[5] The luminescence of trivalent lanthanide ions is a result of transitions within the partially filled 4f shell of the ions. These transitions are parity forbidden leading to low molar absorption coefficients in the order of 10 cm^{-1} and long luminescent lifetimes, up to several milliseconds. These long luminescent lifetimes are advantageous in applications in which population inversions have to be created, such as lasers and optical amplifiers, and for excited state absorption processes, such as up-conversion. There is a growing interest in making optical components in polymer materials because of the easy processing of polymer materials by spin-coating and photolithography.[6] However, in organic media the long-lived excited state of the lanthanide ions is quenched very effectively by the high-energy vibrations of closely spaced organic groups.[7] This is in particular true for the lanthanide ions that emit in the near-infrared, like Er^{3+} and Nd^{3+}, because the energy gap between the luminescent excited state and the ground state is small.[8] Due to this quenching, the pump power has to be very high to reach population inversion. One way of protecting the lanthanide ion from the organic environment is by doping the ions in the core of inorganic nanoparticles. These nanoparticles have

† Current address: University of Victoria, Department of Chemistry, P.O. Box 3065, Victoria, BC, Canada V8W 3V6. E-mail: fvv@uvic.ca.
* Corresponding author.

(1) Brust, M.; Walker, M.; Bethell, D.; Schiffrin, D. J.; Whyman, R. *Chem. Commun.* **1994**, 801.
(2) Murray, C. B.; Norris, D. J.; Bawendi, M. G. *J. Am. Chem. Soc.* **1993**, *115*, 8706.
(3) Blasse, G.; Grabmaier, B. C. *Luminescent materials*; Springer: Berlin, 1994.
(4) (a) Digonet, M. J. F. *Rare earth doped fiber lasers and amplifiers*, 2nd ed.; Marcel Dekker Inc.: New York, 2001. (b) Becker, P. C.; Olsson, N. A.; Simpson, J. R. *Erbium doped amplifiers: fundamentals and technology*; Academic Press: San Diego, CA, 1999.
(5) Reisfeld, R.; Jorgensen, C. K. *Lasers and excited states of rare earths*; Springer: Berlin, 1977.
(6) Slooff, L. H.; van Blaaderen, A.; Polman, A.; Hebbink, G. A.; Klink, S. I.; van Veggel, F. C. J. M.; Reinhoudt, D. N.; Hofstraat, J. W. *Appl. Phys. Rev.* **2002**, *91*, 3955.
(7) (a) Klink, S. I.; Hebbink, G. A.; Grave, L.; Peters, G. A.; van Veggel, F. C. J. M.; Reinhoudt, D. N.; Hofstraat, J. W. *Eur. J. Org. Chem.* **2000**, 1923 and references therein.
(8) (a) Hebbink, G. A.; Reinhoudt, D. N.; van Veggel, F. C. J. M. *Eur. J. Org. Chem.* **2001**, 4101 and references therein. (b) Wada, Y.; Okubo, T.; Ryo, M.; Nakazawa, T.; Hasegawa, Y.; Yanagida, S. *J. Am. Chem. Soc.* **2000**, *122*, 8583.

10.1021/cm034495d CCC: $25.00
Published on Web 10/31/2003

organic groups on the surface and therefore are dispersable in organic solvents, but the ion itself is in an inorganic matrix leading to long luminescent lifetimes. A lot of nanoparticles doped with lanthanide ions have been reported, but most of these particles are made in high temperature processes[9] leading to particles without organic groups on the surface and therefore lacking dispersability in organic solvents. Only a few lanthanide-doped nanoparticles have been reported that are dispersable in organic solvents,[10] but the NIR emitting lanthanide ions have received little attention. For optical telecommunication, particles doped with NIR emitting ions would be of interest, and we have shown that it is possible to dope nanoparticles of $LaPO_4$ with NIR emitting ions such as Nd^{3+}, Er^{3+}, and Pr^{3+} [11] and nanoparticles of LaF_3 with NIR emitting ions such as Nd^{3+}, Er^{3+}, and Ho^{3+}.[12] The particles show NIR emission in organic solvents, and the luminescence lifetimes of the ions are long compared to these ions in solution or in organic complexes. A difference between the two particles is the phonon energy of the host matrix. For $LaPO_4$, the highest phonon energy is around 1050 cm^{-1} while for LaF_3 this is only 350 cm^{-1}.[13] The lower phonon energies of the LaF_3 particles could in principle lead to longer luminescent lifetimes, and this material has been used extensively for a variety of NIR emitting lanthanide ions in the form of crystals and thin films.[14] The luminescence decays of ions doped in these particles were not monoexponential, which was explained by surface effects. In this paper, we will discuss the luminescence properties of these particles in further detail, especially the NIR emitting ions, and propose a model to describe the luminescence decays.[15]

Experimental Section

All chemicals were used as received without further purification. The lanthanide salts were purchased from Aldrich or Acros in the highest purity available (at least 99.9%). Octadecanol (99%), Sodium fluoride (99%), and tris(ethylhexyl)phosphate (98%) were purchased from Fluka, phosphorus pentasulfide (99%) from Aldrich, and trioctylamine (98%) from Acros.

$LaPO_4$ particles were synthesized using a procedure described before.[10] Briefly, 1 mmol of the hydrated $LnCl_3$ (Ln = La^{3+}, Eu^{3+}, Nd^{3+}, Er^{3+}, or Pr^{3+}) is first dissolved in 10 mL of methanol followed by the addition of 6 mL of tris(ethylhexyl)-phosphate and evaporation of the methanol under vacuum. The solution is heated to 70 °C under vacuum to remove water. A solution of 1 mmol of orthophosphoric acid and 3 mmol of trioctylamine in 3 mL of tris(ethylhexyl)phosphate was added, and the reaction mixture was heated at 200 °C under argon. After 40 h, the solution was cooled to room temperature, and methanol was added to precipitate the nanoparticles. The particles were separated by centrifugation and washed two times with methanol. The particles were soluble in methanol by the addition of tetramethylammonium hydroxide. The particles could be precipitated by the addition of ethyl acetate and separated by centrifugation. Particles obtained in this way were surface coated with tetramethylammonium groups and some of the bis(ethylhexyl)phosphate chains.

The ligand ammonium dioctadecyldithiophosphate used in the synthesis of the LaF_3 particles was prepared by heating P_2S_5 (0.02 mol) and octadecanol (0.07 mol) at 75 °C for 3 h. The resulting suspension was cooled to room temperature followed by the addition of dichloromethane and filtration. The solvent was evaporated and the residue taken up in hexane, and ammonia was bubbled through this solution. The resulting precipitate was separated by filtration, washed with hexane, and dried. ^{1}H NMR (DMSO-d_6): δ 7.2−6.9 (broad, 4H), δ 3.7 (dt, J = 8.1, 6.6 Hz, 4H), δ 1.5−1.4 (m, 4H), δ 1.35−1.1 (m, 60H), δ 0.84 (t, J = 6.2 Hz, 6H). MS (MALDI-TOF) m/z = 634.0 $[(M - NH_4^+)^-$, calcd for $C_{36}H_{74}O_2PS_2$: 633.5]; Anal. Calcd for $C_{36}H_{78}NO_2PS_2$: C, 66.31; H, 12.06; N, 2.15; S, 9.83. Found: C, 66.50; H, 12.24; N, 2.27; S, 9.56.

The LaF_3 nanoparticles were prepared by heating a solution of 614 mg (0.95 mmol) of ammonium di-*n*-octadecyldithiophosphate and 126 mg (1 mmol) of NaF in 35 mL of ethanol/water at 75 °C. A solution of $La(NO_3)_3 \cdot 6H_2O$ and $Eu(NO_3)_3 \cdot 6H_2O$ (1.33 mmol total) in 2 mL of water was added dropwise, and the solution was stirred at 75 °C for 2 h and then cooled to room temperature. The precipitate was separated by centrifugation and was washed subsequently with water and ethanol. The particles were further purified by dispersing in dichloromethane and precipitating by the addition of ethanol. After separation by centrifugation, the particles were dried in a vacuum over P_2O_5 for 2 days. After drying the particles, they are soluble in apolar solvents such as chloroform, dichloromethane, and toluene.

TEM images were collected on a Philips CM 30 Twin FTEM, operating at 300 kV. Samples were prepared by evaporating a drop of a diluted particle dispersion, in methanol in the case of $LaPO_4$ and dichloromethane in the case of LaF_3 particles, on a carbon coated 200 mesh copper grid. ^{1}H NMR spectra were recorded at 25 °C on a Varian Inova 300 NMR spectrometer. Elemental analyses were carried out with a model 1106 Carlo-Erbu Strumentazione elemental analyzer. X-ray fluorescence was carried out on a Philips PW 1489 spectrometer using LaF_3, Li_3PO_4, Eu_2O_3, Nd_2O_3, Er_2O_3, Pr_6O_{11}, and Ho_2O_3 as the standards. Infrared spectra were recorded on a FT-IR Perkin-Elmer Spectrum BX spectrometer. Mass spectra were recorded using a Perkin-Elmer/Perspective biosystems Voyager-DE-RP MALDI-TOF mass spectrometer. Photoluminescence measurements in the visible were done with an Edinburgh Instruments FS/FL instrument with a 450 W Xe arc lamp and a red sensitive Peltier element cooled Hamamatsu R955 PMT. The emission spectra were corrected for the detector response, and the excitation spectra were corrected for the lamp intensity. The NIR spectrum of Ho^{3+} was measured with the same instrument using a liquid nitrogen cooled Ge detector. The other NIR spectra were measured by exciting the samples with a CW Ar^+ ion laser operating at 488 nm (Er^{3+}), 476 nm (Pr^{3+}), and 514 nm (Nd^{3+}). The continuous light was modulated with an acousto-optic modulator and focused on the sample in 1 × 1 cm^2 quartz cuvettes. The signal was focused with a 20 cm lens on a monochromator and detected at the monochromator exit with a liquid nitrogen cooled Ge detector (Northcoast) or a PMT (AgOCS) for the spectral region between 700 and 1000 nm. The signal of the detector was fed to a lock-in amplifier. The spectra of the near-infrared emitting ions were measured with a resolution of 6 nm and of the visible emitting ions with a resolution of 0.9 nm.

Luminescence quantum yields were determined by comparing the luminescence intensity of a particle solution with a solution of quinine bisulfate in 1 M H_2SO_4 with approximately

(9) (a) Liu, G. K.; Zhuang, H. Z.; Chen, X. Y. *Nano Lett.* **2002**, *2*, 535. (b) Zych, E.; Hreniak, D.; Strek, W. *J. Phys. Chem.* **2002**, *106*, 3805. (c) Meltzer, R. S.; Feofilov, S. P.; Tissue, B.; Yuan, H. B. *Phys. Rev. B* **1999**, *60*, 14012.

(10) (a) Riwotzki, K.; Meyssamy, H.; Schnablegger, H.; Kornowski, A.; Haase, M. *Angew. Chem., Int. Ed.* **2001**, *40*, 573. (b) Riwotzki, K.; Meyssammy, H.; Kornowski, A.; Haase, M. *J. Phys. Chem. B* **2000**, *104*, 2824.

(11) Hebbink, G. A.; Stouwdam, J. W.; Reinhoudt, D. N.; van Veggel, F. C. J. M. *Adv. Mater.* **2002**, *14*, 1147.

(12) Stouwdam, J. W.; van Veggel, F. C. J. M. *Nano Lett.* **2002**, *2*, 733.

(13) Weber, M. J. *Phys. Rev.* **1967**, *157*, 262.

(14) Payne, S. A.; Chase, L. L.; Smith, L. K.; Kway, W. L.; Krupke, W. F. *IEEE J. Quantum Electron.* **1992**, *28*, 2619.

(15) In ref 10b, Haase and co-workers used a fitting procedure taking into account randomly distributed quenchers located only inside the particles. However, taking into account the large solvent effects on the luminescence lifetimes, it is most likely that most of the quenching takes place from outside the particles and therefore another fitting procedure is needed.

the same absorption at the excitation wavelength of 274 nm. The quantum yield was calculated from the equation $\phi_{sample} = (n^2_{sample} I_{sample} A_{ref} / n^2_{ref} I_{ref} A_{sample}) \phi_{ref}$ with n the refractive index, A the absorption, and I the emission intensity and taking the quantum yield of quinine bisulfate as 54.4%.[16]

Results and Discussion

Characterization. The doping concentration in all particles was 5% of the luminescent ion compared to the total concentration of lanthanide ions, to give a molar ratio of La^{3+}/Ln^{3+} of 19/1, unless stated otherwise. Particles of $LaPO_4$ were synthesized using a literature procedure[10] from the hydrated $LnCl_3$ salts and phosphoric acid. The growth of the particles is controlled by the coordinating solvent tris(ethylhexyl)phosphate and protonated trioctylamine. During the reaction, some of the solvent is hydrolyzed, and the resulting bis(ethylhexyl)phoshate binds to the surface as can be seen by ^{1}H NMR spectroscopy. The LaF_3 nanoparticles were synthesized using ammonium dioctadecyldithiophosphate as ligand. To a solution of this ligand and NaF in a water/ethanol mixture was added dropwise a solution of the $Ln(NO_3)_3$ salts in water. The dithiophosphate headgroup of the ligand coordinates weakly to the lanthanide ions allowing the growth of the nanoparticles but coordinates strongly enough to keep the particles from aggregating.[17] The particles were characterized using TEM by evaporating a drop of particle dispersion on a carbon coated copper grid. Typical pictures for LaF_3:Ln and $LaPO_4$:Ln (Ln = Eu^{3+} and Nd^{3+}) are shown in Figure 1.

The morphologies of both particles are independent of the dopant ion. The high crystallinity of the particles can clearly be seen, despite the fact that the particles were synthesized at relatively low temperatures, i.e., below 200 °C. The $LaPO_4$ particles with an average size of 4.3 nm are somewhat smaller in size than the LaF_3 particles with an average size of 6.3 nm. In addition, the size distribution of 15% for the $LaPO_4$ particles is lower than the size distribution of the LaF_3 particles, which is 28%. The LaF_3 particles are less spherical in shape with aspect ratios between 1 and 3. The spherical and elongated particles both consist of one crystal domain, so the elongated particles are not formed by the aggregation of multiple particles. In the size distribution histograms, the sizes of the elongated particles were determined by averaging of the long and the short axes. The sizes of both particles are sufficiently small to prevent scattering when the particles are incorporated in a polymer matrix.[18]

The elemental composition of the particles was determined using X-ray fluorescence (XRF) and combustion elemental analysis. The results are summarized in Table 1.

The same ratio of lanthanide ions as applied in the synthesis was found in the particles reflecting the similar reactivity of the lanthanide ions. The rest

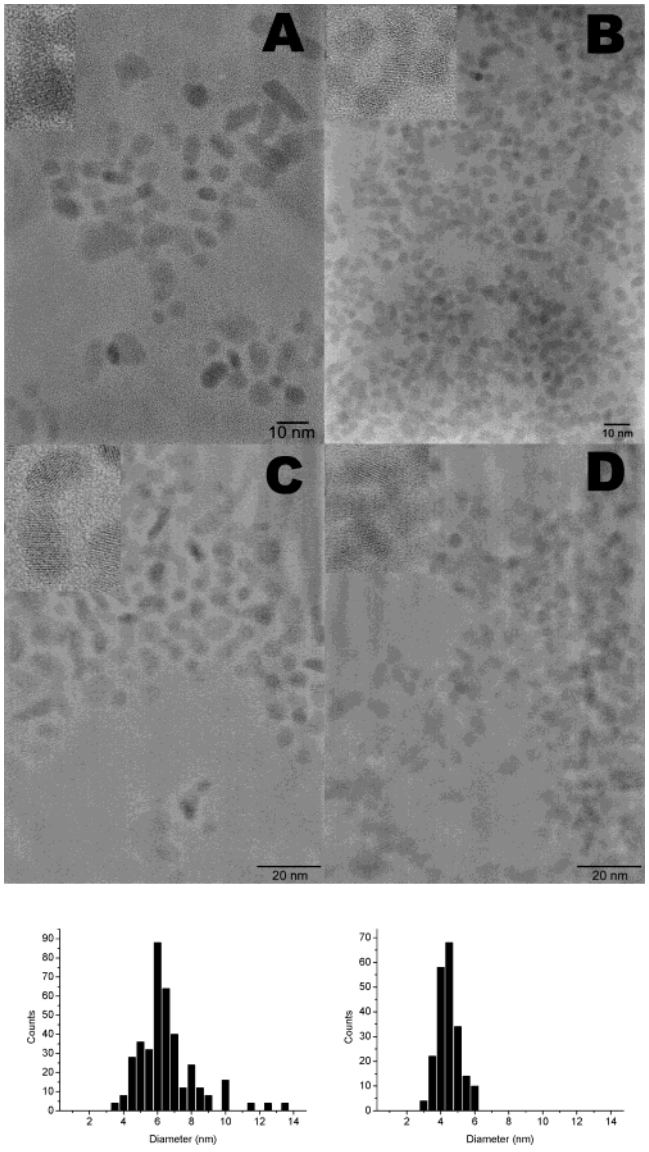

Figure 1. TEM pictures of (A) LaF_3:Eu, (B) $LaPO_4$:Eu, (C) LaF_3:Nd, and (D) $LaPO_4$:Er particles with the size distribution histograms of LaF_3:Ln and $LaPO_4$:Ln particles. The insets show magnifications of some particles. The sizes of the nonspherical particles were determined by averaging the long and the short axes.

Table 1. Elemental Composition of the Particles (wt %)

particle	La[a]	Ln[a]	P[a]	C[b]	N[b]	H[b]	S[b]
$LaPO_4$:Nd	41.97	2.42	12.19	6.33	1.01	2.16	
$LaPO_4$:Er	41.80	2.36	12.56	5.57	1.20	2.63	
$LaPO_4$:Pr	43.30	2.35	12.52	6.30	1.01	2.17	
LaF_3:Nd	17.81	0.86	11.23	42.49		7.76	5.76
LaF_3:Er	17.41	0.81	11.25	43.59		7.62	6.48
LaF_3:Ho	25.47	1.17	9.50	33.07		5.88	5.72

[a] XRF. [b] Combustion elemental analysis.

consists of organic groups on the outside of the particles such as tetramethylammonium ions and ethylhexyl chains for the $LaPO_4$ particles and the coordinated dithiophosphate ligands for the LaF_3 particles. The surfaces of the $LaPO_4$ nanoparticles consist of deprotonated phosphate groups coordinated to ammonium ions and some of the solvent and hydrolyzed products of the solvent. The coordination of the organic molecules can be seen from the broadened signals in the ^{1}H NMR and the ratio of Ln/P, that is smaller than one, indicates that

(16) Eaton, D. F. *Pure Appl. Chem.* **1988**, *60*, 1107.

(17) When the stronger coordinating phosphate ligand was used, no particles were formed, only the complex of the lanthanide ion with the ligand. The coordination of this ligand is apparently too strong to allow particle growth.

(18) Scattering is dependent on the particle size and the difference in refractive index between the particles and the polymer. Providing that the nanoparticles do not aggregate in a polymer film, a size of 10 nm is sufficiently small to minimize scattering.

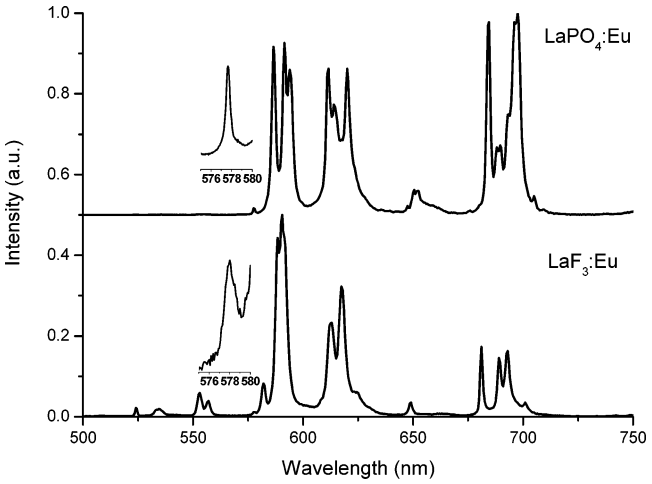

Figure 2. Emission spectra of LaF_3:Eu (λ_{ex} 397 nm) and $LaPO_4$:Eu (λ_{ex} 260 nm) particles. The insets are magnifications of the $^5D_0 \rightarrow {}^7F_0$ emissions, measured at 0.1 nm resolution.

phosphate groups are at the surface and not the lanthanide ions. For the LaF_3 particles, it is likely that the surface consists of Ln^{3+} ions, because these can coordinate to the negatively charged ligand that stabilizes the particle. The coordination of the ligand to the surface of the particles can be seen from the broadened signals of the ligand in the ^1H NMR spectrum. Fluoride could not be detected using both these analysis techniques so no information could be obtained about the amount of F in the LaF_3 particles. The amount of ligand measured with elemental analysis on the LaF_3 particles is not always constant. For the Nd^{3+} and Er^{3+} doped particles, the amount of carbon and hydrogen measured is the same, but the amount of sulfur is slightly lower for the Nd^{3+} particles. A deviation in the amount of sulfur could be caused by oxidation of the ligand after prolonged exposure to air, as found by mass spectrometry. This oxidation leads to a ligand with a phosphate headgroup, which binds more strongly to the particles and would therefore lead to even more stable particles. For the Ho^{3+} doped particles, the amount of carbon and hydrogen is lower than for the other two ions. The particle size and size distribution is the same as for the other two batches, so apparently there is less ligand coordinated to the Ho^{3+} doped particles. For all these particles, no free ligand is present because no nitrogen was detected and because only broadened signals are present in the ^1H NMR spectra proving the coordination of the ligand to the particle surface. Surface properties of nanoparticles usually play an important role in the luminescence properties, and it is therefore important to know which molecules are coordinated to the surface.

Luminescence of Eu^{3+}-Doped Particles. The Eu^{3+} ion was used as a probe for the crystal environment in which the ion is located. Typical Eu^{3+} emission originating from the $^5D_0$ and $^5D_1$ levels was observed after direct excitation of the ion at 397 nm for LaF_3:Eu and 260 nm for $LaPO_4$:Eu (Figure 2).

In $LaPO_4$, the Eu^{3+} can be excited at 260 nm because of a charge transfer band. This charge transfer band is visible in more phosphors in which Eu^{3+} is coordinated to oxygen and is caused by an electron transfer in the $Eu^{3+}-O^{2-}$ bond. Deactivation of the charge transfer state leads to an excited Eu^{3+} ion. Due to the low reduction potential of Eu^{3+}, this band occurs at wavelengths above 200 nm. In the emission spectrum, the ratio of the different peaks of the $^5D_0 \rightarrow {}^7F_J$ ($J = 1, 2$) transition gives information about the symmetry of the crystal site in which the ion is located. This confirms that the dopant ion is present in a La^{3+} crystal site giving the Eu^{3+} ion C_1 symmetry in $LaPO_4$ and C_2 symmetry in LaF_3 particles, the same as for the bulk materials.[19,20] In the LaF_3:Eu particles, emission from the $^5D_1$ level at 524, 534, 554, and 582 nm can clearly be observed as well. Emission from this level also occurs in the $LaPO_4$:Eu particles only with much less intensity. This large difference in emission from the $^5D_1$ level is caused by the difference in phonon energies of the host materials. The $^5D_1$ level lies only 1750 cm^{-1} above the $^5D_0$ level, and thus, the $^5D_1$ level can be depopulated very fast to the $^5D_0$ level by multi-phonon emission in $LaPO_4$. In the LaF_3 host, the maximum phonon energies are so low that multi-phonon emission becomes inefficient. The different symmetry sites of Eu^{3+} in these particles can clearly be observed from the different emission spectra. The Eu^{3+} ion can also be used as a probe for more similar crystal structures as is illustrated in $LnPO_4$ nanoparticles with Ln = La, Gd, Y, and Lu, synthesized using the same procedure described for $LaPO_4$ particles. The crystal structure of these phosphates is dependent on the size of the lanthanide ion. A monazite type is found for the larger lanthanide ions ($Ln = La^{3+}-Gd^{3+}$) and xenotime for the smaller lanthanide ions ($Ln = Tb^{3+}-Lu^{3+}$).[21] The excitation and emission spectra for $LnPO_4$:Eu ($Ln = La^{3+}$, Gd^{3+}, Y^{3+}, Lu^{3+}) nanoparticles are shown in Figure 3.

The excitation spectra are scaled to the 393 nm peak of Eu^{3+}, and all show a charge transfer band, but the excitation maximum is blue shifted upon a decrease in ion size. The excitation spectra of $LuPO_4$ and YPO_4 exhibit a sharp cutoff around 220 nm, which is caused by the absorption of the excitation light by the solvent. The blue shift of the charge transfer band upon decreasing the ion size can be explained by a stronger binding of the phosphate groups to the smaller trivalent ions and by the smaller crystal site the Eu^{3+} ion has in the $LuPO_4$ and YPO_4 lattices. This makes the phosphates more difficult to oxidize and the reduction of Eu^{3+} to Eu^{2+} less favorable. The sharp lines in the $GdPO_4$ host at 273, 276, and 278 nm and some smaller peaks around 310 nm are due to the excitation of Gd^{3+} ($^8S_{7/2} \rightarrow {}^6I_J$, ^6P_J, $J = {}^3/_2$, ${}^5/_2$, and ${}^7/_2$) and subsequent energy transfer to the Eu^{3+} excited states. The emission spectra of all four $LnPO_4$:Eu materials exhibit the characteristic Eu^{3+} emission lines for the $^5D_0 \rightarrow {}^7F_J$ ($J = 0-4$) transitions. Some differences are observed in the emission spectra of the two host materials with the larger ions (La^{3+} and Gd^{3+}) compared to the host materials with the smaller ions (Y^{3+} and Lu^{3+}). The relative intensities of the $^5D_0 \rightarrow {}^7F_2$ transition are different: 0.30, 0.30, 0.43, and 0.50 for the doped $LaPO_4$, $GdPO_4$, $LuPO_4$, and YPO_4, respectively. These values correspond to a crystal site with a high degree of inversion symmetry and more inversion symmetry for the La and Gd phosphates than for the Lu and Y phosphates. Furthermore, a number of extra

(19) Ropp, R. C. *J. Electrochem. Soc.* **1968**, *115*, 841.
(20) Carnall, W. T.; Goodman, G. L.; Rajnak, K.; Rana, R. S. *J. Chem. Phys.* **1989**, *90*, 3443.
(21) Rambabu, U.; Buddhudu, S. *Opt. Mater.* **2001**, *17*, 401.

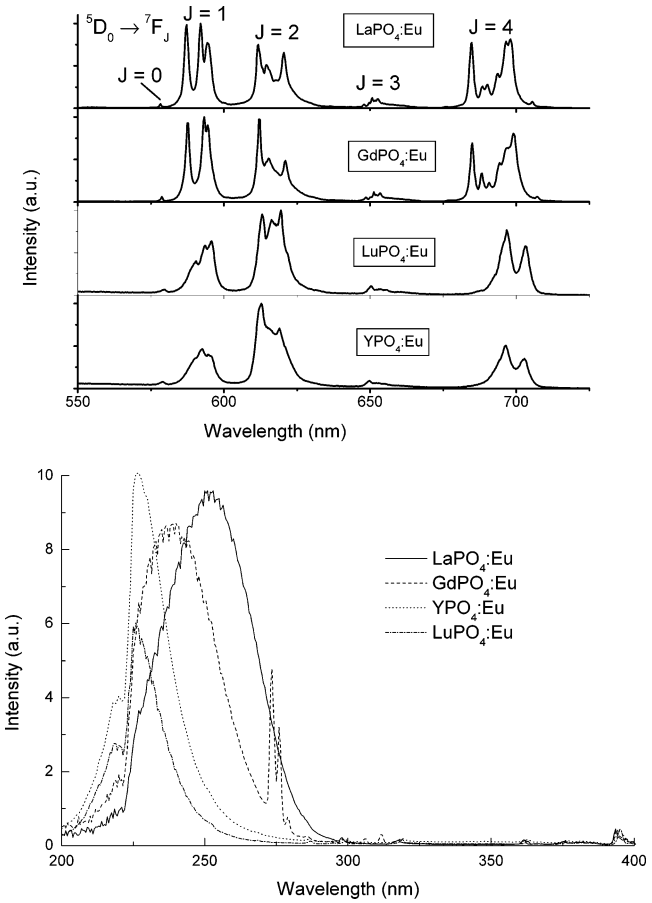

Figure 3. Normalized emission, λ_{ex} 250 nm, (top) and excitation (bottom) spectra of $LnPO_4$:Eu particles in methanol. The excitation spectra (λ_{em} 612 nm) are normalized on the 393 nm excitation peak of Eu^{3+}.

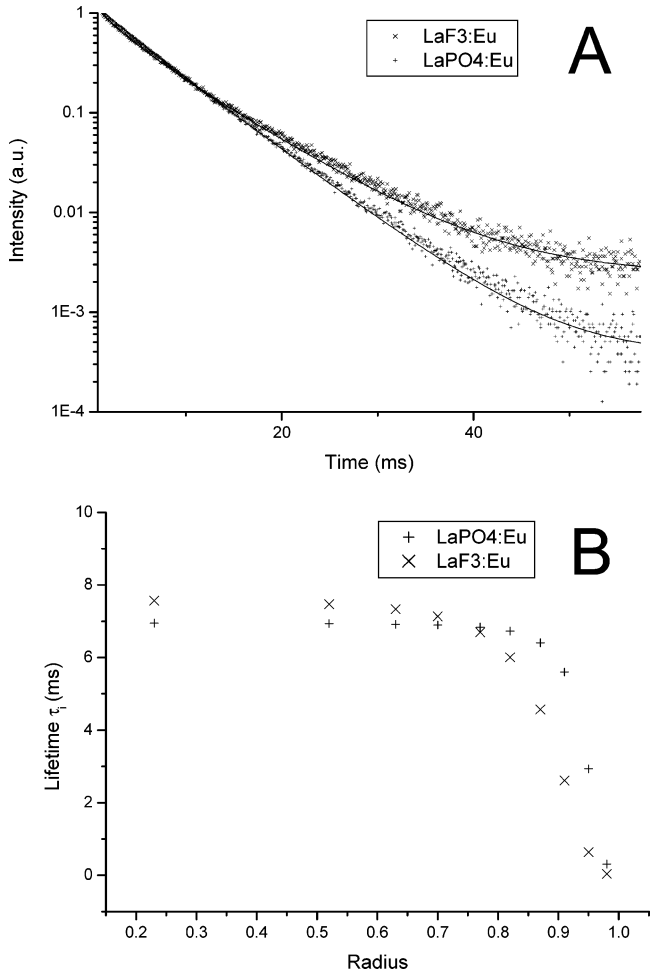

Figure 4. Luminescence decays (top) of LaF_3:Eu (λ_{ex} 397) in dichloromethane and $LaPO_4$:Eu (λ_{ex} 260 nm) in methanol, collecting the emission at 591 nm. The fits were obtained by using the model described in the text. The bottom picture shows the distribution of the lifetimes over the particle axis.

peaks are found in the $^5D_0 \rightarrow {}^7F_4$ transition, all consistent with the difference in crystal structure between the $LaPO_4$, $GdPO_4$ and the $LuPO_4$ and YPO_4 particles.

The luminescence decay of the ion gives information on the influence of quenching from the organic solvent and ligand outside the particle and quenching by impurities from inside the particle. An example of the decays of LaF_3:Eu and $LaPO_4$:Eu particles is given in Figure 4a.

Excitation occurs in the higher lying Eu^{3+} levels followed by a rapid decay to the luminescent $^5D_0$ level. For the $LaPO_4$:Eu particles, the luminescence of the $^5D_0$ level shows a short rise with a time constant of 24 μs. This is similar to the decay time of the $^5D_1$ level of 23 μs showing that the $^5D_0$ level is partially populated through the $^5D_1$ level. After this short rise in the $LaPO_4$:Eu luminescence, both decays are clearly not monoexponential, so not all ions in the particles have the same probability of decay. An acceptable fit was obtained when two exponentials were used.[22] However, there is no physical reason to use just two exponentials. Quenching by groups close to or at the surface of the nanoparticle should lead to a gradual change of quenching efficiency of the lanthanide ion from the surface to the core of the particle. Assuming a random distribution of the dopant lanthanide ion over the nanoparticle and that all ions are in the same crystal site, there is no physical justification for fitting the decay curve with just two exponentials, which suggests two populations. A random distribution of the doping ions is reasonable because of the high similarity in cation size, charge, and reactivity between the lanthanide ions. It was possible to check if all the ions are in the same crystal site. First of all, the emission of the $^5D_0 \rightarrow {}^7F_0$ transition gives information on the amount of crystal sites the ion is doped in. This is a transition between two nondegenerate levels, so if all the ions are in the same crystal site, only one emission peak for this transition is present around 578 nm. In both Eu^{3+} doped particles of LaF_3 and $LaPO_4$, we indeed see just one peak for this transition, measured at a resolution of 0.1 nm (inset Figure 2), indicating that all ions are in the same crystal site. Time-resolved spectroscopy is another method giving information on different crystal sites. Ions doped in different crystal sites have a different symmetry leading to a difference in emission spectrum and a difference in luminescent lifetime. An emission spectrum taken directly after an excitation pulse is caused

(22) Using a biexponential fit for the luminescence decay, lifetimes for LaF_3:Eu particles in CH_2Cl_2 are 7.7 ms for the long component, contributing 74% to the total luminescence and 2.9 ms for the short component, contributing 26% to the total luminescence. For $LaPO_4$:Eu particles in methanol, values of 6.4 ms for the long component, contributing 57% to the total luminescence, and 3.4 ms for the short component, contributing 43% to the total luminescence, were obtained.

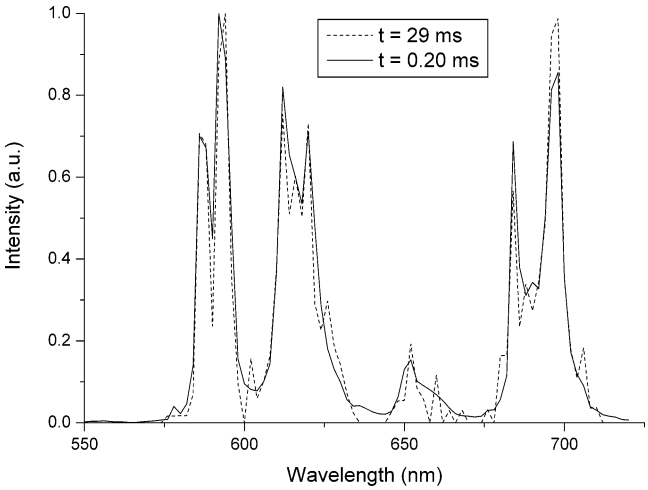

Figure 5. Time-resolved emission spectra of $LaPO_4$:Eu in methanol with a delay of 0.2 and 29 ms after the excitation pulse.

by emission from both types of ions, but an emission spectrum at the end of the decay is the emission from ions with the longest lifetime. When all ions are in the same crystal site, no differences in emission spectrum should be observed. Figure 5 shows the emission spectra of $LaPO_4$:Eu in methanol 0.2 ms after an excitation pulse and 29 ms after an excitation pulse.

Although the intensity at the end of the decay is much lower, the shape of the emission spectrum is essentially the same as in the early stages of the decay, thereby confirming that Eu^{3+} is doped in one single crystal site.

Modeling the Luminescence Decay. When it is assumed that most of the quenching of the excited state is located close to the surface, a model can be designed taking into account these surface effects. Ions in the core of the particles will have the longest lifetime, and going to the outside the lifetime will decrease. When a particle is divided into a number of shells, the lifetime of one shell can be related to the lifetime in another shell by an effective radiative lifetime and a quenching factor that is dependent on the distance to the surface. The luminescence decay can thus be described using eq 1.[23]

$$I_t = I_0 \sum_{i=1}^{n} \frac{1}{n} e^{-k_i t};\ k_i = \frac{1}{\tau_i} = k_R + C \times f_{q,i} \qquad (1)$$

In this equation, I_t is the luminescence intensity at time t, I_0 the intensity at $t = 0$, n the number of shells, $k_i = 1/\tau_i$ the rate constant in shell i, with τ_i the luminescent lifetime of this shell, t the time, $k_R = 1/\tau_R$ a rate constant in the absence of quenching from outside the particle so it is an apparent radiative decay rate, and C the quenching constant. The value of k_R is an apparent decay rate, because it only takes into account quenching from the surface. All other quenching processes inside the nanoparticle, like concentration quenching and quenching by impurities inside the nanoparticle, can also be present. The constant C is a fit parameter that is dependent on the individual ion, the size and size distribution of the particles, and on the strength of the quenching. The size and size distribution are still in the quenching constant, because at this moment no size dependent decays are available. The relative quenching factor $f_{q,i}$ takes into account the distance of a shell to the surface and the distance dependence of the quenching. When quenching is assumed to take place via a dipole−dipole mechanism, the quenching has a distance dependence of r^{-6}.[24] The total quenching then has to be integrated over the total volume outside the particle. Integration over the total volume gives the total quenching factor $f_{q,i}$ (eq 2).

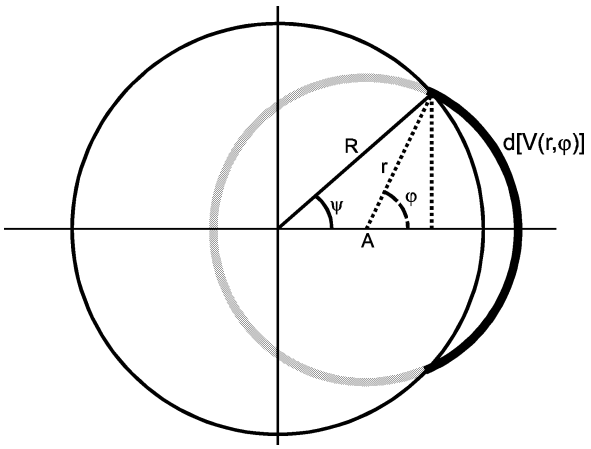

Figure 6. Schematic representation of a particle and the representation of the symbols used in the text.

$$f_{q,i}(a_i) = \int_V r^{-6}\, dV \qquad (2)$$

This equation was solved for a particle shell i, with $a_i = A_i/R_i$ as the center of each shell, by varying the radius r (Figure 6). Three domains can be defined. The first domain is totally inside the particle ranging from $r = 0$ to $r = (R - A)$, so for this domain no quenching is taken into account. In the second domain, the volume fraction $d[V(r,\varphi)]$ is dependent on both the radius and the angle φ (part of the shell is inside the particle with no quenching and part is outside the shell, but with quenching). This domain ranges from $r = (R - A)$ to $r = (R + A)$ (Figure 6).

The third domain lies totally out of the particle and is from $r = (R + A)$ to ∞. The fraction of a shell in the second domain that is outside the particle equals $2\pi r^2$-$(1 - \cos \varphi)dr$. The volume fraction dV of a shell in the third domain is $4\pi r^2\, dr$. Multiplying this with r^{-6} results in the following integral (eq 3), that was numerically solved for a particle consisting of 10 shells[25] of equal volume. Assuming that the ions are randomly distributed in the particle will give all ions the same weight in the fit.

$$f_{q,i}(A,\varphi) = \int_V r^{-6}\, dV = \int_{R-A}^{R+A} \frac{1}{r^6} 2\pi r^2 (1 - \cos\varphi) dr + \int_{R+A}^{\infty} \frac{1}{r^6} 4\pi r^2\, dr \qquad (3)$$

(23) In this approach, we neglect the $^5D_1$ emission from Eu^{3+} (typical lifetime of this level in LaF_3:Eu is 2.5 ms and 25 μs in $LaPO_4$:Eu). The contribution to the total emission is about 5% in the case of LaF_3:Eu and close to zero in the case of $LaPO_4$:Eu.

(24) Ermolaev, V. L.; Sveshnikov, E. B. *Russ. Chem. Rev.* **1994**, *63*, 905.

(25) The choice to take 10 shells is an arbitrary choice. Fitting with 6 shells gave the same results, but more shells could increase the accuracy of the fit.

Table 2. Quenching Factor $f_{q,i}$ for 10 Shells

shell i	a_i	$f_{q,i}(a_i)$
1	0.23	4.9
2	0.52	11
3	0.63	19
4	0.70	32
5	0.77	63
6	0.82	121
7	0.87	3.0×10^2
8	0.91	8.6×10^2
9	0.95	4.9×10^3
10	0.98	7.7×10^4

This results in relative quenching factors for the different shells as shown in Table 2.

Using these values for the quenching factors, the decays of the particles can be fitted by varying the values for the apparent radiative lifetime τ_R and C. Good fits were obtained for $LaPO_4$:Eu and LaF_3:Eu particles (Figure 4a, —). In these fits, the luminescence of the $^5D_1$ level is not taken into account. Emission from this level contributes only very little to the total emission, but it could have a small influence on the obtained values.

For $LaPO_4$:Eu particles in methanol, the value for τ_R is 7.0 ms with a quenching constant of 4.1×10^{-2} s^{-1}. In the case of LaF_3:Eu particles in dichloromethane, the τ_R is 7.7 ms with a quenching constant of 2.9×10^{-1} s^{-1}. These results show that the apparent radiative lifetime of Eu^{3+} in LaF_3 is longer than that in $LaPO_4$ from the literature,[26,27] but that the ion is quenched more strongly in the LaF_3 particles than in the $LaPO_4$ particles. The difference in solvent does not explain the difference in quenching strength, because methanol is a stronger quenching solvent than dichloromethane due to the presence of an O−H bond. The different termination of the surface could be the reason for a different quenching strength. The $LaPO_4$ particles are terminated with phosphate groups, but the LaF_3 particles are terminated with Ln^{3+} groups. This means that in the case of LaF_3 particles the luminescent ion can directly coordinate to a quenching group of the organic environment or the ligand, which is not the case for the $LaPO_4$ particles. One other possible source of quenching is the coordination of water to the surface of the particles. It has been shown that the lifetime of LaF_3:Eu particles is longer when the particles are synthesized in deuterated solvents[12] proving that residual OH groups are present after the synthesis and act as quenchers. When this product was stirred in a water/methanol mixture, the lifetime of Eu^{3+} went back to the value for particles synthesized in nondeuterated solvent, proving that the OH groups are at the surface of the particles and accessible to the solvent. The $LaPO_4$ particles are synthesized under near water free conditions, and any water present will be used in the hydrolysis of the solvent, so contamination with water is probably less important. The apparent radiative lifetimes ($\tau_R = 1/k_R$) do not necessarily relate to the real radiative lifetime, because quenching inside the particle is not taken into account in this model. However, the high values do indicate that quenching inside the particle is not significant. The size dispersity of the particles is in the quenching constant C, so the values of C for LaF_3 and $LaPO_4$ particles cannot be compared directly with each other. Figure 4b shows the variation of the lifetime τ_i in the different particle shells. As expected, the longest lifetimes are observed in the core of the particles, and going to the surface of the particles the lifetime decreases consistent with quenching by the solvent. Because the total luminescence is the area under the decay curve, an average lifetime of these 10 values can be calculated using eq 4.

$$\tau_{av} = \frac{\sum A_i \tau_i^2}{\sum A_i \tau_i} \tag{4}$$

For LaF_3:Eu, an average lifetime of 6.5 ms is calculated, and for $LaPO_4$:Eu particles, an average lifetime of 6.6 ms. The values for these materials are close to the radiative lifetimes calculated and measured previously for the bulk materials,[26,27] but unfortunately, it is not possible to compare them directly to these radiative lifetimes, because the nanoparticles are in another solvent. However, they do indicate a high quantum yield.

Quantum Yield. A quantum yield of these lanthanide-doped particles can be determined using Ce^{3+} doped particles.[28] Ce^{3+} has a high absorption between 200 and 300 nm because of an allowed 4f−5d transition. It is known that Ce^{3+} shows efficient energy transfer to Tb^{3+}, which emits in the visible and from particles doped with both these ions, it is possible to determine the quantum yield by comparison with a dye. We determined the quantum yield by using quinine bisulfate in 1 M H_2SO_4 as standard. For $La_{0.4}Ce_{0.45}PO_4Tb_{0.15}$, a quantum yield of 10% in methanol was found, lower than the value of 24% found by Haase and co-workers.[10a] The value found by Haase et al. was measured using Rodamine 6G, and when we used this dye, a quantum yield of 21% was found, which is within the experimental error of about 2% (absolute). The value found using quinine bisulfate is probably more reliable, because this dye is more suitable for excitation in the UV.[29] The Rodamine 6G dye has a low absorption at the excitation wavelength and much overlap between emission and absorption, so at higher concentration, reabsorption of emission could occur leading to an overestimation of the quantum yield. The emission and absorption of quinine bisulfate have very little overlap so self-quenching at higher concentrations does not take place. It was also possible to synthesize $La_{0.4}Ce_{0.45}F_3Tb_{0.15}$ particles, and the emission spectrum is shown in Figure 7 together with the emission spectrum of quinine bisulfate.

For $La_{0.4}Ce_{0.45}F_3Tb_{0.15}$ in dichloromethane, a quantum yield of 19% was found. When D_2O was added to a dichloromethane solution of $LaCeF_3Tb$ particles, an increase in quantum yield to 38% was observed. This confirms the coordination of a small amount of water to the surface of the particles leading to quenching of the excited state of the lanthanide ions. The high-energy

(26) Weber, M. J. In *Optical properties of ions in crystals*; Crosswhite, H. M., Moose, H. W., Eds.; Interscience: New York, 1967; p 467.

(27) Dexpert-Ghys, J.; Mauricot, R.; Faucher, M. D. *J. Lumin.* **1996**, *69*, 203.

(28) Due to the low absorption of the lanthanide ions, it is difficult to determine the optical density of a particle solution, and it is therefore not possible to compare the emission with the emission of a dye with a known quantum yield.

(29) Demas, J. N.; Crosby, G. A. *J. Phys. Chem.* **1971**, *75*, 991.

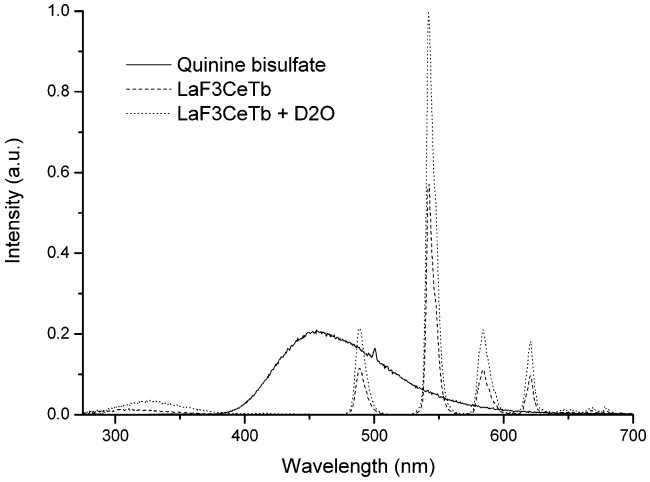

Figure 7. Emission spectra of LaF_3:Ce,Tb particles in CH_2Cl_2 and quinine bisulfate dissolved in 1 M H_2SO_4 (λ_{ex} 282 nm).

vibrations of water molecules effectively quench the excited state of the lanthanide ions, and this can be reduced by an exchange with deuterium because of the lower vibrational energy of the OD bond.[30] This coordination of water is in full agreement with previous results,[12] where particles of LaF_3:Eu were synthesized in deuterated solvents, leading to an increase in the luminescence lifetime.

Near-Infrared Emission. Particles of $LaPO_4$ and LaF_3 were also doped with the NIR emitting ions Nd^{3+}, Er^{3+}, Pr^{3+}, and Ho^{3+}. Luminescence spectra of these ions are shown in Figure 8.

The luminescence spectra of Nd^{3+} in both particles show the typical emission at 880, 1060, and 1330 of the $^4F_{3/2} \rightarrow {}^4I_{13/2}$, $^4F_{3/2} \rightarrow {}^4I_{11/2}$, and $^4F_{3/2} \rightarrow {}^4I_{9/2}$ transitions, respectively. The emission spectrum measured for LaF_3:Nd looks very similar to the spectrum measured in a Nd^{3+}-doped LaF_3 thin film.[31] The emissions are almost the same for both types of particles, showing only slightly different splitting of the emission peaks, indicative of a different symmetry around the luminescent ion, like that found for the Eu^{3+} ion. However, the differences in the luminescence spectra are smaller than for Eu^{3+}, because Eu^{3+} is much more sensitive to the symmetry of the crystal site than the other lanthanide ions.[32] The excitation spectra for both particles also look very similar and are comparable with the absorption lines of the Nd^{3+} ion in solution.[33] The wavelength positions of the peaks do not change, only the peak splitting and the ratio between peak intensities differ. Er^{3+}-doped materials show typical luminescence at 1530 nm of the $^4I_{13/2} \rightarrow {}^4I_{15/2}$ transition in both particles with a small difference in the shape and the width of the emission peak caused by a difference in crystal symmetry. The emission of the LaF_3:Er particles again looks very similar to the emission spectrum of an Er^{3+}-doped LaF_3 thin film.[34] For the $LaPO_4$ host, also a small emission is observed at 980 nm of the $^4I_{11/2} \rightarrow {}^4I_{15/2}$ transition, which is not visible in the LaF_3 host, probably because of symmetry reasons. The excitation spectra are very similar for both particles, showing small differences in peak intensities caused by symmetry differences. For the Pr^{3+} ion, luminescence can originate from different levels depending on the crystal field and on the quenching mechanisms.[35] Luminescence originating from the $^1D_2$ level was observed in $LaPO_4$:Pr particles by excitation with the 476 nm line of an Ar^+ laser. When the LaF_3:Pr particles were excited using the same laser line, no emission was observed, although it is known that the Pr^{3+} ion can emit very efficiently in this host matrix.[36] It is possible that Pr^{3+} does not absorb at this wavelength in the LaF_3 host or that the Pr^{3+} ion is very sensitive to the small amount of water present at the surface of the LaF_3. Under excitation with an Xe arc lamp at 443 nm, the emission of $LaPO_4$:Pr could also be detected, but only weak emission was observed for LaF_3:Pr particles. For the Ho^{3+} ion, emission could be detected in the LaF_3:Ho particles at 960 and 1460 nm from the $^5F_5 \rightarrow {}^5I_7$ and $^5F_5 \rightarrow {}^5I_6$ transitions. In the visible, an emission of the $^5F_5 \rightarrow {}^5I_8$ transition at 640 nm was also observed (not shown). In this host, Ho^{3+} luminescence is known to occur from a variety of levels.[37] The dominant luminescence found in the bulk material is from the $^5S_2$ level at 540 nm, which is, however, not observed in our nanoparticles. A reason for this can be that this level lies approximately 3000 cm^{-1} above the $^5F_5$ level which corresponds to the vibrational energy of a CH bond. The presence of the ligands on the surface of the particle could lead to a fast nonradiative decay of the $^5S_2$ level to the $^5F_5$ level from which luminescence occurs. The $LaPO_4$:Ho particles did not show any luminescence at all. Ho^{3+} emission in $LaPO_4$ crystals is not reported in the literature probably because the phonon energies in $LaPO_4$ are too high, leading to relatively efficient nonradiative processes. NIR emission of Pr^{3+} and Ho^{3+} in an organic environment has not been reported till now, proving the good shielding against the organic groups when they are doped in the nanoparticles. Using these ions the spectral window between 1300 and 1600 nm, which is of interest to telecommunication purposes, can be covered completely.

Yb^{3+} as a Sensitizer. To increase the effective absorption of the Er^{3+} ion, codoping with Yb^{3+} is often used.[38] Yb^{3+} has a higher absorption at 980 nm than Er^{3+}, and it is able to transfer energy to the Er^{3+} ion. The 980 nm wavelength is commonly used for pumping Er^{3+} ions because at this wavelength a large variety of cheap semiconductor pump lasers are available. Yb^{3+} also has a low reduction potential leading to charge transfer bands in phosphates, similar to Eu^{3+},[39] so the possibility of a charge transfer in $LaPO_4$ particles was investigated. The emission and excitation spectra of a sample of $LaPO_4$:Yb in methanol are shown in Figure 9.

(30) Holz, R. C.; Chang, C. A.; Horrocks, W. DeW., Jr. *Inorg. Chem.* **1991**, *30*, 3270.
(31) Bhutta, T.; Chardon, A. M.; Shepherd, D. P.; Daran, C.; Serrano, C.; Munoz-Yague, A. *IEEE J. Quantum Electron.* **2001**, *37*, 1469.
(32) Kirby, A. F.; Richardson, F. S. *J. Phys. Chem.* **1983**, *87*, 2544.
(33) Heller, A. *J. Am. Chem. Soc.* **1967**, *89*, 167.
(34) Buchal, C.; Siegrist, T.; Jacobson, D. C.; Poate, J. M. *Appl. Phys. Lett.* **1996**, *68*, 438.
(35) Nishida, Y.; Yamada, M.; Kanamori, T.; Kobayashi, K.; Temmyo, J.; Sudo, S.; Ohishi, Y. *IEEE J. Quantum Electron.* **1998**, *34*, 1332.
(36) Hegarty, J.; Huber, D. L.; Yen, W. M. *Phys. Rev. B* **1982**, *25*, 5638.
(37) Caspers, H. H.; Rast, H. E. *J. Chem. Phys.* **1970**, *53*, 3208.
(38) Strohhöfer, C.; Polman, A. *J. Appl. Phys.* **2001**, *90*, 4314.
(39) Nakazawa, E. *J. Lumin.* **2002**, *100*, 89.

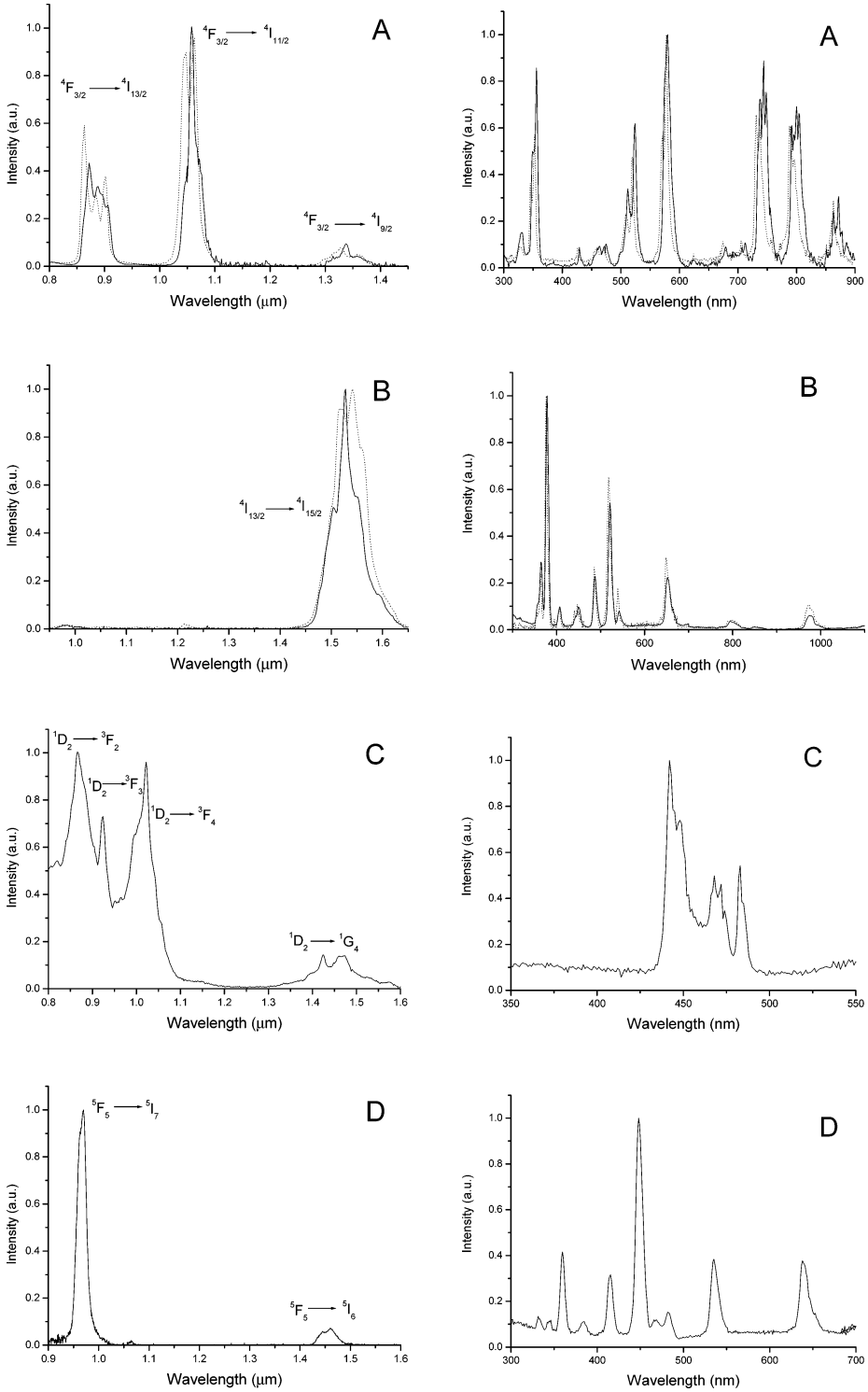

Figure 8. Emission (left) and excitation (right) spectra of (A) LaF_3:Nd (···), $LaPO_4$:Nd (—); (B) LaF_3:Er (···), $LaPO_4$:Er (—); (C) $LaPO_4$:Pr; and (D) LaF_3:Ho. The LaF_3 particles were dissolved in CH_2Cl_2 and the $LaPO_4$ particles in methanol-d_4. The emission spectra of the Nd^{3+} doped particles were collected after excitation at 514 nm and the excitation spectra by collecting the emission at 1060 nm. The Er^{3+} doped particles were excited at 488 nm, and the emission was measured at 1530 nm. For Pr^{3+} and Ho^{3+}, the excitation was at 476 and 448 nm, respectively, and the emission at 730 and 966 nm, respectively.

In the excitation spectrum, a broad band peaking at 250 nm observed. Excitation of the sample at this wavelength leads to typical Yb^{3+} emission peaking at 980 nm. The only excited 4f level of Yb^{3+} is the $^2F_{5/2}$ level, so the broad band at 250 nm is caused by charge transfer excitation. The peak of this charge transfer emission is blue shifted compared to Eu^{3+} reflecting the higher reduction potential of Yb^{3+} compared to Eu^{3+}.[39]

The emission and excitation spectra of $LaPO_4$ particles codoped with Yb^{3+} and Er^{3+} both at 5% are shown in Figure 10.

The absorption lines of Er^{3+} and a broad band peaking at 250 nm are visible in the excitation spectrum. The presence of this broad band is caused by charge transfer excitation of Yb^{3+} followed by energy transfer to Er^{3+}. When the sample was excited in the broad band at 250

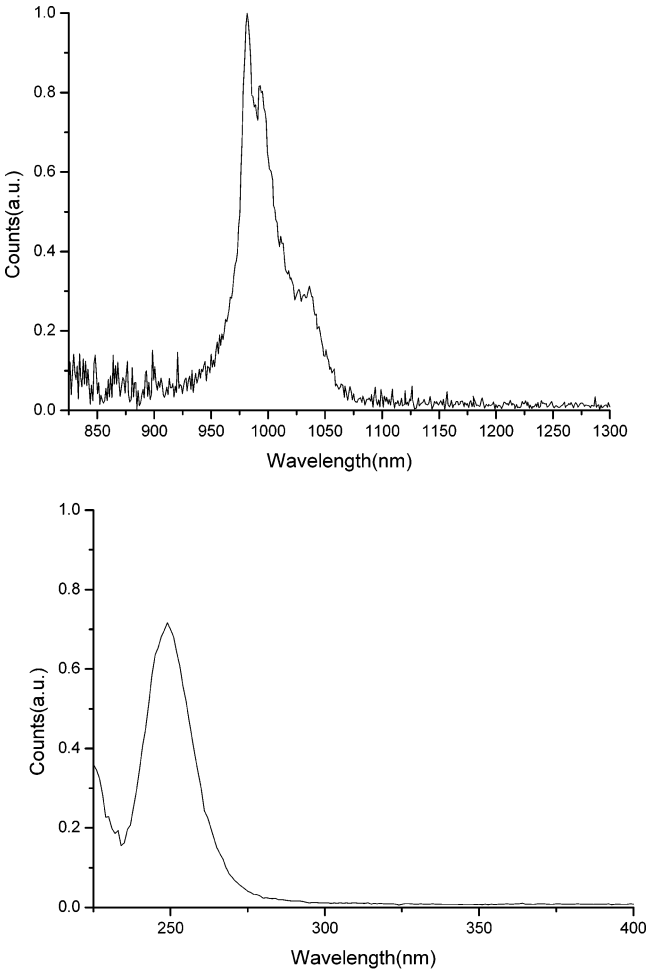

Figure 9. Emission (top) and excitation (bottom) spectra of $LaPO_4$:Yb particles in methanol.

nm, emission at 980 nm from Yb^{3+} and at 1530 nm from Er^{3+} was observed. The appearance of Yb^{3+} emission means that energy transfer is not complete. The direct excitation of Er^{3+} at 378 nm leads to Er^{3+} emission at 1530 nm as expected, but also Yb^{3+} emission at 980 nm is observed, showing that energy transfer from Er^{3+} to Yb^{3+} is also possible. This reverse process needs phonon energy from the surroundings because the $^4I_{11/2}$ energy level of Er^{3+} lies a bit lower in energy than the $^2F_{5/2}$ level of Yb^{3+}. In LaF_3 particles, energy transfer between Yb^{3+} and Er^{3+} is also observed after direct excitation of Yb^{3+} into the $^2F_{5/2}$ level around 980 nm. In this matrix, no charge transfer band is observed, similar to Eu^{3+}. Particles of LaF_3 codoped with various amounts of Yb^{3+} and 5% of Er^{3+} were synthesized, and the luminescence properties were determined in order to optimize the energy transfer.

The emission spectra of LaF_3 particles doped with a varying amount of Yb^{3+} and 5% Er^{3+} excited at 940 nm are shown in Figure 11. The emission spectra are normalized to the Yb^{3+} emission. Excitation at 940 nm was chosen because Er^{3+} has no absorption at this wavelength, so all emission from Er^{3+} is formed through sensitized emission by Yb^{3+}. At 1530 nm, Er^{3+} emission is clearly observed, proving the energy transfer between the ions. The Yb^{3+} emission at 980 nm is still dominating, so energy transfer is not complete. By increasing the amount of Yb^{3+}, the relative Er^{3+} emission increases, so the energy transfer becomes more efficient

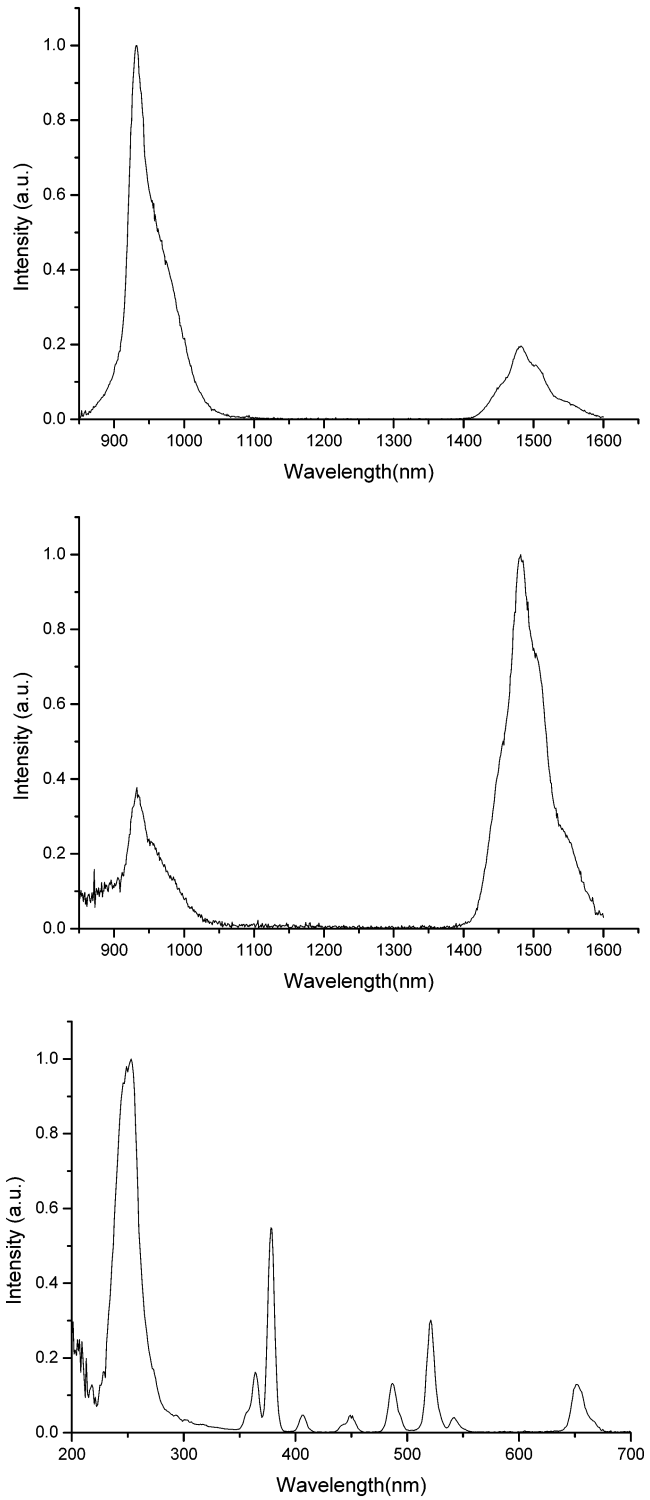

Figure 10. Emission λ_{ex} 250 nm (top) and λ_{ex} 378 nm (middle) spectra of $LaPO_4$:Yb,Er particles in methanol. The bottom picture shows the excitation spectrum of the same sample collecting the emission at 1530 nm.

up to a doping concentration of 20% Yb^{3+} where the maximum energy transfer is reached. Increasing the concentration of Yb^{3+} above 25% does not increase the energy transfer further. At increasing Yb^{3+} concentration, the energy transfer becomes more efficient because the average distance between the ions decreases. It levels off when all the Er^{3+} ions have at least one Yb^{3+} ion as the nearest neighbor.[40] The excitation spectra of Er^{3+} luminescence at 1530 nm for samples doped with

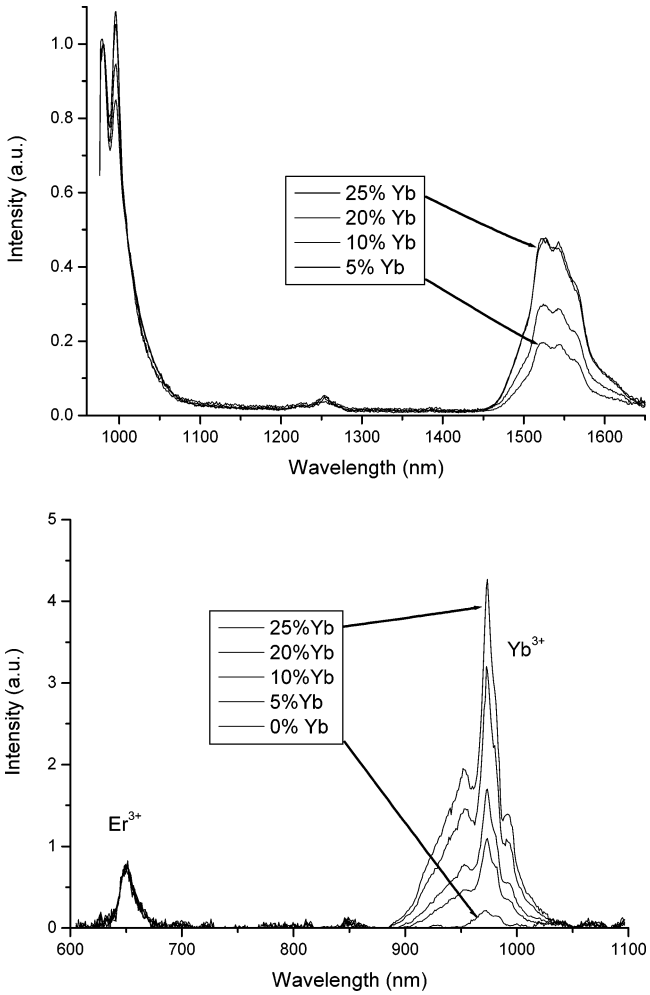

Figure 11. Emission spectra (top) and excitation spectra (bottom) of LaF_3:Yb,Er with 5% Er^{3+} and different amounts of Yb^{3+}. The particles were dissolved in CH_2Cl_2.

different amounts of Yb^{3+} are also shown in Figure 11. The excitation spectra are scaled to the Er^{3+} absorption peak at 650 nm, because the amount of Er^{3+} in the sample is constant. It can be seen that the excitation peak of Er^{3+} in the sample *without* Yb^{3+} around 980 nm is very low and that it can be increased by codoping with Yb^{3+}. Increasing the amount of Yb^{3+} leads to a linear increase of the Yb^{3+} peak compared to the Er^{3+} peak, because more energy is absorbed by Yb^{3+} ions. It was reported in the literature that energy transfer from Yb^{3+} to Er^{3+} in Y_2O_2S nanoparticles is less efficient than in bulk material, because of the absence of low energy phonons.[41] These low energy phonons are required to take up the small energy released when the excitation energy is transferred from Yb^{3+} to Er^{3+}. In the present case, in which the nanoparticles are capped with organic molecules, these low energy phonons are present in the form of vibrational and rotational energies, thus facilitating a more efficient energy transfer.

Decays of Near-Infrared Emitting Ions. Luminescence decays of NIR emitting ions could also be fitted using the described model. Some decays with fits are shown in Figure 12, and Table 3 gives the values of the fit constants τ_R and C.

The luminescence lifetimes reported for Er^{3+} and Nd^{3+} are very long compared to values reported previously in an organic environment.[11,12] An increase in the luminescence lifetime by a factor of 10−1000 is observed. For Nd^{3+}, the values of the average lifetime and τ_R are higher for LaF_3 than for $LaPO_4$ reflecting the difference in the phonon energies of the matrices. This is the other way around for Er^{3+}. Both the value of τ_R and the average lifetimes are lower for the LaF_3:Er particles compared to the $LaPO_4$:Er particles. Not only the quenching is stronger, but the lower τ_R indicates that there are more quenching possibilities for Er^{3+} remaining inside the particles. This could be a result of the higher reaction temperature for the $LaPO_4$ particles, which functions as a better annealing step compared to the LaF_3 particles. The average lifetimes of Pr^{3+} and Ho^{3+} are in the microsecond range reflecting the shorter radiative lifetimes of these ions. For Pr^{3+} in a phosphate host, a lifetime of 70 μs for the $^1D_2$ level was reported in the literature,[42] and for Ho^{3+} in LaF_3, a lifetime of the $^5F_5$ level of 780 μs was calculated.[43]

Using the described model, different factors influencing the luminescence lifetimes of these particles were investigated. Er^{3+} usually shows a large dependence on the doping concentration, and when the particles are doped with different concentrations of Er^{3+}, this is indeed reflected in the values of τ_r and C (Table 4).

A decrease in Er^{3+} concentration should not change the quenching constant C because the Er^{3+} ions are still in the same crystal site and at the same average distance to the surface. The value of τ_R should increase with a decreasing doping concentration because quenching processes such as cross-relaxation and up-conversion become less important.[44] This is clearly observed in the fitted values for LaF_3:Er with different Er^{3+} concentrations. A pronounced increase in τ_R is observed when the concentration is lowered, while C stays about the same for the concentrations used here. For the $LaPO_4$:Er particles, the constant C does change and becomes lower at a lower doping concentration. The different surface termination of the particles can play a role here. One quenching path is the transfer of the excitation energy of ions in the core of the particles to ions closer to the surface followed by quenching. This process is dependent on the concentration of the doping ion, because energy transfer becomes more efficient at higher doping concentrations, but also on the surface termination. In the LaF_3 particles, lanthanide ions are coordinated directly to the ligand and other possible quenchers, but in the case of the $LaPO_4$ particles, PO_4 groups are at the surface.

In addition, quenching by solvents with a different quenching strength can be described using this model. Fit values obtained for $LaPO_4$:Nd and $LaPO_4$:Eu in

(40) Manssmann, M. *Z. Kristallogr.* **1965**, *122*, 375.
(41) Liu, G. K.; Zhuang, H. Z.; Chen, X. Y. *Nano Lett.* **2002**, *2*, 535.
(42) Lian, R.; Yin, M.; Zhang, W.; Lou, L.; Krupa, J. C. *J. Alloys Compd.* **2000**, *311*, 97.
(43) Weber, M. J.; Matsinger, B. H.; Donlan, V. L.; Surrat, G. T. *J. Phys. Chem.* **1972**, *57*, 562.
(44) In cross-relaxation processes, the energy of a highly excited state of an ion is transferred to a neighboring ion in the ground state promoting it to an excited state. This process can be positive leading to two ions in the right excited state or negative leading to two ions in the wrong levels. In up-conversion, two ions in the excited state couple in a way that when one ion decays to the ground state it transfers its energy to the other ion promoting it to a higher excited level. This can lead to the emission of a photon of higher energy or to nonradiative decay to the first excited level.

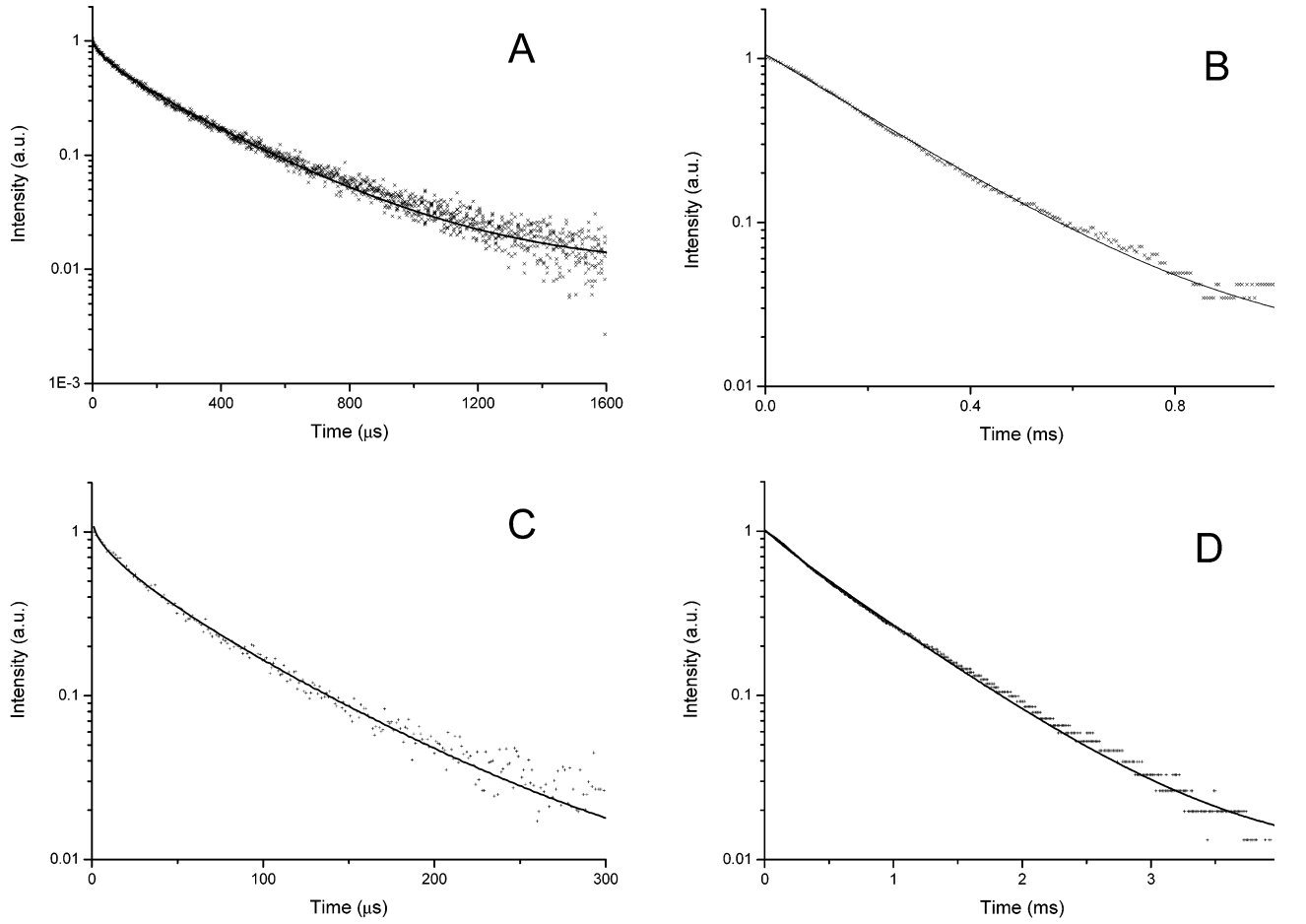

Figure 12. Luminescence decay curves of (A) LaF_3:Nd, (B) LaF_3:Er, (C) $LaPO_4$:Nd, and (D) $LaPO_4$:Er particles dissolved in CH_2Cl_2. The Nd^{3+} doped particles were excited with the 514 nm line of an Ar^+ laser, and the emission was collected at 1060 nm. The Er^{3+} doped particles were excited with the 488 nm line of an Ar^+ laser, and the emission was collected at 1530 nm. The solid lines represent the fits using the model described in the text.

Table 3. Fit Parameters for the NIR Emitting Ions in the Two Different Particles[a]

particle	solvent	τ_R (μs)	C (s^{-1})	τ_{av} (μs)
$LaPO_4$:Nd	CD_3OD	90	107	68
LaF_3:Nd	CH_2Cl_2	347	23.5	265
$LaPO_4$:Er	CD_3OD	315	4.66	304
LaF_3:Er	CH_2Cl_2	236	3.29	226
$LaPO_4$:Pr	CD_3OD	4.0	57.3	3.7
LaF_3:Ho	CH_2Cl_2	35	27	31

[a] All doping concentrations were 5%. The errors in τ_R are ≈3% and in C ≈10% determined from duplicate measurements.

Table 4. Fit Parameters for LaF_3:Er and $LaPO_4$:Er at Different Doping Concentrations[a]

	LaF_3:Er		$LaPO_4$:Er	
concentration	τ_R (μs)	C (s^{-1})	τ_R (μs)	C (s^{-1})
5%	236	3.29	315	4.66
2%	332	3.73	758	4.27
1%	465	3.54	1070	2.92

[a] The errors in τ_R are ≈3% and in C ≈10% determined from duplicate measurements.

methanol with a different degree of deuteration are given in Table 5.

For all particles, the same τ_R is found in agreement with the fact that the particle itself does not change. The C constants are different, as expected. A small quenching constant is found for the Eu^{3+} ions, because the energy gap of Eu^{3+} is relatively large and it is

Table 5. Fit Parameters for $LaPO_4$:Nd and $LaPO_4$:Eu in Methanol with Different Degrees of Deuteration[a]

	Nd^{3+}		Eu^{3+}	
solvent	τ_R (μs)	C (s^{-1})	τ_R (ms)	C (s^{-1})
CH_3OH	87	733	7.0	4.06×10^{-2}
CH_3OD	91	214	6.9	1.18×10^{-2}
CD_3OD	90	107	6.9	1.31×10^{-2}

[a] The errors in τ_R are ≈3% and in C ≈10% determined from duplicate measurements.

therefore less sensitive to quenching. In nondeuterated methanol, the strongest quencher is the OH group, and replacing this with an OD group leads to a large decrease in C. Replacement of the CH group by CD leads to another small decrease in quenching in the case of Nd^{3+}, but in the case of Eu^{3+}, the effect is negligible, consistent with the larger energy gap between the excited state and the ground state for Eu^{3+}.

One factor not included in the model is the difference in refractive index between the core and the surrounding solvent. The radiative lifetime of the lanthanide ion is dependent on the refractive index of the surroundings, and it was previously found that particles in solvents with a different refractive index show a different luminescence lifetime.[12,45] The average lifetime for LaF_3:Eu particles dissolved in different solvents increased

(45) Tissue, B. M. *Chem. Mater.* **1998**, *10*, 2837.

from 6.1 ms in a refractive index of 1.525 to an average lifetime of 7.3 ms in a solvent with a refractive index of 1.352. The effect of the refractive index on the luminescence lifetimes of a biexponential fit was primarily seen on the long component of the two lifetimes, not on the short one. The short component is mostly determined by surface quenching, and for this reason, the effect of the refractive index on the results of the model will be small, except for changing the τ_R.

Another refinement of the model will be to take into account the size and size distribution of the particles. The size and size distribution are currently taken up by the constant *C*, averaging all the sizes in one batch. By taking into account the size and size distribution, we could look systematically at the effect of different particle sizes on the luminescent lifetime.

Conclusions

Nanoparticles of LaF_3 and $LaPO_4$ doped with luminescent trivalent lanthanide ions that are dispersable in organic solvents were prepared. These nanoparticles show typical lanthanide luminescence characteristic of the ions doped in the respective bulk material. The luminescence lifetimes of the ions are somewhat lower than for the bulk material, but the lifetimes are much longer compared to lanthanide ions previously measured in solution and in organic complexes. The increase in the luminescence lifetimes shows the effective shielding from the organic environment by the particle. Due to this increase in luminescence lifetime, they are promising materials for applications where population inversion is required like lasers and optical amplifiers, or where excited state absorption is required in processes such as up-conversion. The luminescence lifetimes are not monoexponential, and a model has been proposed to explain this in terms of quenching by groups outside the particles. With this model, factors influencing the luminescence lifetime, like concentration quenching, and quenching by the solvent, can be described. With the model, the deviation from monoexponential behavior is described in terms of surface quenching and not in terms of two distinct populations, which is the case for a biexponential fit.

Acknowledgment. This research is supported by the Council of Chemical Sciences of The Netherlands Organization for Scientific Research (NWO-CW).

CM034495D